J. Phys. B: Atom. Molec. Phys., Vol. 6, January 1973. Printed in Great Britain.

Formation of HCO^+ by the associative ionization of CH + O

Malcolm MacGregor† and R Stephen Berry

Department of Chemistry and The James Franck Institute, The University of Chicago, Chicago, Illinois 60637, USA

MS received 22 May 1972

Abstract. The cross section and rate constant of the chemi-ionization reaction $CH + O \rightarrow HCO^+ + e$ are calculated from a theoretical model. The treatment assumes that the collision partners follow classical adiabatic trajectories up to the region where the potential surfaces cross, and that either the Landau–Zener model or a unit probability gives the transition probability for curve-crossing along the single dimension defined by the trajectory. Potential surfaces were obtained from a combination of experimental data and INDO calculations. Cross sections and rates were computed for a variety of parameters, in order to test their sensitivity to the model. The process can proceed from CH + O in their ground states; of the available potential surfaces of neutral HCO, the most important is that of the $^2\Sigma^-$ state, followed by the two surfaces associated with the $^2\Delta$ state. The cross section for the $^2\Sigma^-$ surface may be as high as 8 Å^2 for collisions of very low velocity. The rate coefficient curve deemed most probable gives values of ca. $3{\cdot}5 \times 10^{-11}$ cm^3 s^{-1} at 1000 K, and about 7×10^{-12} cm^3 s^{-1} at 25 K.

1. Introduction

Ionization may be produced by the collision of two neutral atomic or molecular species, at relative kinetic energies well below typical ionization energies. Such ionization processes are often called 'chemi-ionization' processes. Chemi-ionization has been invoked as a major mechanism in flames and shocks and may play a role in the formation of polyatomic species in interstellar space. Our purpose here is to study the reaction cross section and rate coefficient, as yet unmeasured, for the most probable primary chemi-ionization reaction in hydrocarbon–oxygen mixtures, the reaction of oxygen atoms with CH radicals. This class of reactions, in which the heavy particles remain together and only an electron goes free, is an example of *associative* ionization, $A + B \rightarrow AB^+ + e$.

The past twelve years have seen a great deal of work on the problem of ionization in hydrocarbon flames. There is fairly good agreement on the reaction mechanism involved in production of ionization in flames. The evidence is based on mass spectrometric studies (Fontijn *et al* 1965) and Langmuir probe techniques. (Lawton and Weinberg 1964, Peeters and van Tiggelen, 1969). This mechanism is:

$$CH + O \rightarrow HCO^+ + e^- \quad (1)$$

$$HCO^+ + H_2O \rightarrow H_3O^+ + CO \quad (2)$$

$$H_3O^+ + e^- \rightarrow H_2O + H \quad (3)$$

† Present address: Naval Research Laboratory, Washington, D.C. 20390

where HCO^+ is the primary chemi-ion even though H_3O^+ is the predominant ionic species in most flames.

Reaction (1) is also apparently the primary ion-forming reaction in shock-heated gas systems. (Matsuda and Gutman 1970.) We would also suggest reaction (1) may be an attractive candidate for the formation of polyatomic molecules in interstellar space. The presence of HCO^+ has already been proposed to account for one signal in the radio spectrum. (Klemperer 1970, Buhl and Snyder 1970.)

Although the chemi-ionization reaction $CH + O \rightarrow HCO^+ + e^-$ is fairly generally accepted as the primary ion-forming process, the rate (Bascombe *et al* 1962, Peeters *et al* 1969) is relatively unknown. It is our purpose to investigate, theoretically, the microscopic mechanism of this reaction in terms of electronic states and potential surfaces, and to calculate the cross section of reaction (1) as a function of collision energy, and its rate constant as a function of temperature.

2. Model

Our investigation has been a semi-empirical theoretical study. From the observed spectra of HCO (Johns *et al* 1960, Shirk and Pimentel 1968, Milligan and Jacox 1969), the potential energy curves (Dressler and Miescher 1965) of the isoelectronic NO and NO^+, the recently determined heat of reaction, 4 kcal/mole, for reaction 1 (Matthews and Warnek 1969, Chupka 1972, private communication, the results essentially confirm the value obtained by Warneck) and calculations of the potential energy surfaces of HCO and HCO^+ by the INDO method, we have attempted to infer the most probable process leading to the formation of HCO^+ in thermal collisions with CH and O.

The potential energy surfaces for the ground states of HCO and HCO^+, in the region of their minima, were calculated by the INDO molecular orbital method (Pople and Beveridge 1970). The potential surfaces of the excited states of HCO were obtained from the ground state eigenvalues by a small extension of a method due to Huzinaga (Huzinaga and Arnau 1970, 1971). We are particularly concerned with finding the shapes of specific surfaces of HCO^+ and excited HCO, and with locating the crossings of the potential surface of the ion with those of the neutral radical.

The INDO method has been described in detail, and needs no further discussion, but it is probably useful to discuss Huzinaga's treatment of excited states. Huzinaga proposed a method to obtain meaningful excited-state orbitals from molecular Hartree–Fock calculations. The procedure consists of constructing an operator $\mathbf{V} = (1 - \mathbf{P})\mathbf{\Omega}(1 - \mathbf{P})$ from the results of a molecular orbital calculation of the molecular ground state, where P is the projection operator $\Sigma_{i \subset \text{occupied}} |\psi_i\rangle\langle\psi_i|$ and Ω is an arbitrary hermitian operator chosen to adjust the potential to represent the field in which the 'excited' electron moves. If ψ_i is expanded in terms of the finite basis set of atomic orbitals $\{\chi_i\}$,

$$\psi_i = \sum_{p=1}^{n} c_{ip}\chi_p$$

as in the Roothaan method, and we define the matrices **D** and **S**,

$$D_{pq} = \sum_{j \subset \text{occupied}} c_{jp}c_{jq}$$

$$S_{pq} = \langle\chi_p|\chi_q\rangle$$

then **V** may be expressed as

$$\mathbf{V} = \mathbf{\Omega} - (\mathbf{\Omega DS} + \mathbf{SD\Omega}) + \mathbf{SD\Omega DS}.$$

Huzinaga (Huzinaga and Arnau 1971) applied this procedure to the zero-differential overlap approximation using $\mathbf{\Omega} = aJ_i + bK_i$. We have extended his procedure to the intermediate neglect of differential overlap (INDO) approximation for an open shell system using the same matrix $\mathbf{\Omega}$.

Once **V** is calculated, the new orbitals are obtained from the new hamiltonian $\mathbf{F}+\mathbf{V}$, where **F** (in our case, $\mathbf{F}^\alpha$ or $\mathbf{F}^\beta$) is the final Hartree–Fock matrix derived by iteration to self-consistency. We solve the equation

$$(\mathbf{F}+\mathbf{V})\mathbf{C}_v = \epsilon_v \mathbf{S}\mathbf{C}_v$$

to obtain a new set of virtual orbital energies, ϵ_v. With these virtual orbital energies, the excited state energies E^{ex} may be calculated directly from the ground state energy E^{gs} as

$$E^{ex} = E^{gs} + \epsilon_j - \epsilon_i$$

for the excitation of an electron from the original state i to the new virtual orbital j. We attempted to apply this method to two-electron excitations with less than satisfactory results, probably due to the compressed nature of the atomic orbitals used in the INDO approximation.

The cross section for reaction from any selected initial channel was obtained by an impact parameter method similar to one introduced by Tully and Preston for the reaction of H^+ with D_2 (Tully and Preston 1971). We assume that the relative motion of CH and O is governed by the classical equations of motion on the particular potential surface for the channel in question. We make the approximation that the rotation and vibration of CH can be neglected, on the ground that the dominant contribution to the transition probability comes from a very narrow range of O–CH distance. This assumption thus corresponds to neglecting any orientational forces or adiabatic bond-stretching forces of O on CH. One of the most natural refinements of our treatment would be in the inclusion of orientation forces and of the CH rotation. However, with rotation and reorientation neglected, it becomes quite straightforward to compute the trajectory for a single O–CH collision when the initial impact parameter, velocity and orientation are chosen. Finding the transition probability for that particular collision is thus reduced from a multidimensional surface-crossing problem to a one-dimensional curve-crossing problem in which the potential *curves* are defined by that section through the multidimensional surface determined by the particular reaction trajectory. This reduction gives, the transition probability P_α from the Landau–Zener–Stueckelberg method (Landau and Lifshitz 1958, Stueckelberg 1932, Zener 1932) or an estimate of the *upper limit* of the cross section and rate, by using the assumption that the transition probability for ionization is unity for all trajectories that reach the crease of intersection of the ionic surface with the surface for the incident state. Both assumptions were pursued in this work. As we have applied the LZS model, the transition probability takes on nonzero values only in the immediate regions of the surface crossings, corresponding to the assumption that the electron can only leave with the minimum amount of kinetic energy allowed by the shapes of the surfaces. This assumption is almost certainly too strong, so that the LZS model, in effect, gives cross sections and rate coefficients that tend to be lower limits to the actual values. The LZS and unit probability models thus are intended to bracket the real cross sections and rate coefficients.

The cross section for the particular α-channel, σ_α, is then obtained by averaging the transition probability over the orientation ω of CH relative to the collision axis and integrating over impact parameter b. The total cross section σ is obtained by averaging over incident channels (weighted by their statistical probabilities). The rate coefficient is found from the average of the product of cross section and velocity, taken with a Boltzmann distribution of velocities. Thus

$$\sigma_\alpha(v) = \int\int P_\alpha(b, v, \omega) b \, db \, d\omega,$$

$$\alpha(v) = \sum G_\alpha \sigma_\alpha(v)$$

and

$$k(T) = \int \alpha(v) \exp(-mv^2/2kT) v \, dv.$$

Calculation of the transition probabilities for curve crossing using the LZS theory is subject to rather severe approximations. The LZS theory and corrected versions (Coulson and Zalewski 1962) hold for exothermic processes where the energies are much larger than the energy difference between the adiabatic curves at the crossing. Therefore the theory becomes inadequate as we approach a thermoneutral reaction. The length of the coupling distance, and the shape of the colliding pairs, can give rise to errors in calculating the probability (Bates 1960), although the validity of the Landau–Zener expression seems to extend to a far wider class of situations than was once thought (Olson *et al* 1971).

The transition probability p, for transition from one curve to another in a single passage, according to the LZS theory is given by

$$p = \exp\left(\frac{-2\pi}{\hbar v} \frac{|\epsilon_{12}(R_0)|^2}{|F_1 - F_2|}\right)$$

where v is the relative radial collision velocity, F_i, is the slope of the potential energy curve, $F_i = \partial V_i/\partial R$, and $\epsilon_{12}(R_0)$ is the interaction energy of the two states at the crossing point R_0. Since ionization is an irreversible process and we are looking for the likelihood that it happens either on the incoming or the outgoing part of the trajectory, the probability P_i of associative ionization, expressed in terms of the probability p of adiabatic passage through the crossing is $P_i = (1-p)+p(1-p) = (1-p^2)$.

3. Results and discussion

By far the most important path for the reactive collision occurs via the ground state reactants $CH(x^2\Pi)$ and $O(^3P)$, whether one is concerned with a reaction in interstellar space (Klemperer 1970, Buhl and Snyder 1970) or in hydrocarbon flames (Peeters 1971). At one time, it was thought that reaction (1) was endothermic and that excited states of CH or O or both were required if the reaction were to occur in ordinary thermal systems. However, the latest determinations of the heat of formation of the HCO^+ ion (Matthews and Warneck 1969, Chupka 1972) make it fairly certain that the reaction is exothermic by about 4 kcal/mole and that only the ground-state reactants are required. The combination of $CH(x^2\Pi)$ and $O(^3P)$ gives rise to the molecular states $^{4,2}\Sigma^+$, $^{4,2}\Sigma^-$, $^{4,2}\Delta$ and $^{4,2}\Pi$ in the linear configuration of HCO. Of these states, only the doublets will interact with the $^1\Sigma^+(^1A')$ ground state of HCO^+ if the spin conservation

rule is obeyed. We assume that this is the case. The $^2\Pi$ is the ground state of linear HCO. On bending, the $^2\Pi$ splits into $^2A'$ and a $^2A''$. The $^2A''$ state does not cross the ground state potential energy surface of HCO^+. The remaining doublet states, $^2\Sigma^-(^2A'')$, $^2\Sigma^+(^2A'')$ and $^2\Delta$ (two A' states) all intersect the $HCO^+(^1A')$ state and can contribute to the transition probability. Actually, the $^2\Delta$ (both $^2A'$ states) which crosses the HCO^+ potential energy surface has the form of the excited $CH(A^2\Delta)+O(^3P)$ configuration, but an adiabatic avoided crossing arises with the two components of the $^2\Delta$ state from the $CH(X^2\Pi)+O(^3P)$ configuration.

Sections through the potential energy surfaces for HCO and HCO^+ are presented as functions of R(C–O) at HCO angles of 180° and 140° in figures 1 and 2 for the $^2\Delta$, $^2\Sigma^+$ and $^2\Sigma^-$ states (and the corresponding $^2A'$ and $^2A''$ states) respectively. In figures 3 and 4, the $^2\Delta$ and $^2\Sigma^+$, $^2\Sigma^-$ states are shown as function of the HCO angle for the two R(C–O) distances 1·00 Å and 1·30 Å. These energy surfaces were calculated from the evaluation of energy points determined on a grid of four distances (R(C–O) = 1·07, 1·17, 1·27 and 1·37) and five angles (∠HCO = 180°, 170°, 150°, 130° and 110°). In the calculation of the higher-energy $^2\Delta(^2A')$ state by Huzinaga's method, a two-electron excitation was required but, because of the ground state nature of the INDO atomic orbitals, an unreasonably low energy resulted. However, the *shape* of the surface was similar to that obtained with virtual orbitals. To correct for the low energy, the whole surface was moved up and bent slightly for R(C–O) ~ 1·4 Å, to meet the other $^2\Delta(^2A')$ (single excitation) state in the linear configuration. As it turns out, the required amount of bending was very small.

A comparison of our theoretical results and the experimental results (Shirk and Pimentel 1968, Dixon 1969) are in agreement as far as the structure is concerned. Our configuration for the $^2\Pi(^2A')$ ground state is R(C–O) = 1·23 Å, ∠HCO = 125° and R(C–H) = 1·16 Å (held fixed) as compared to the experimental R(C–O) = 1·17 Å

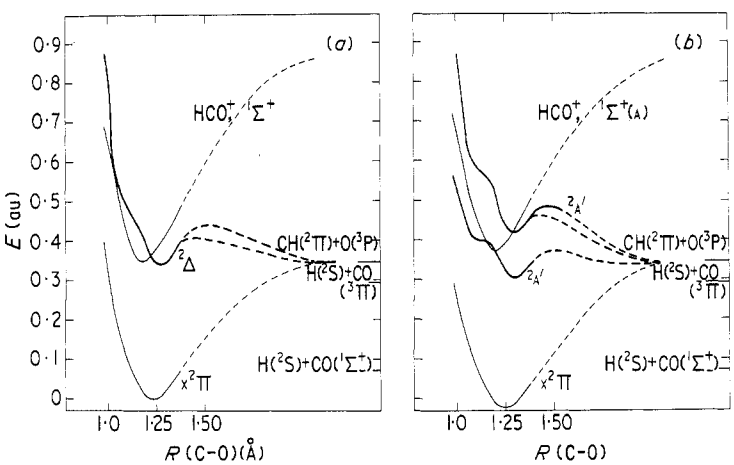

Figure 1. Sections through the potential surfaces, showing the ground states of HCO and HCO^+, and (*a*) the $^2\Delta$ excited state of linear HCO and (*b*) the two $^2A'$ states, into which the $^2\Delta$ splits, when the HCO angle is 140°. Calculations were made for portions of the curves drawn solid; dashed sections were arbitrarily drawn to connect the calculated curves to the correct dissociation limits. Calculations were carried out with two different choices for the arbitrary curves; these were intended to represent lower and reasonable upper limits for the activation barriers; in the low-barrier case, the barrier drops to zero when the HCO angle reaches some undetermined angle in the vicinity of 150°.

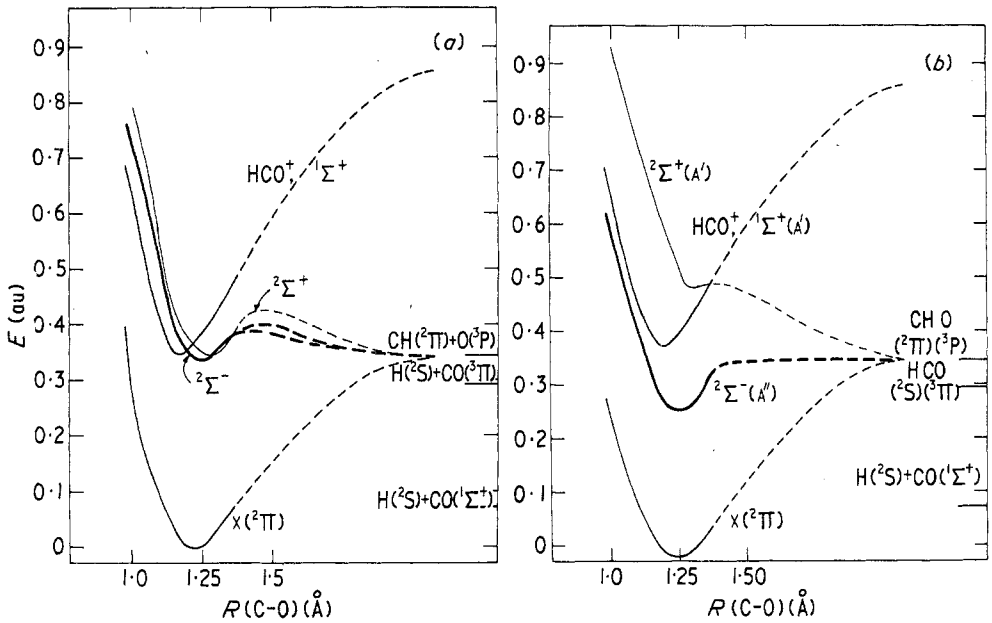

Figure 2. Sections through the potential surfaces showing the $^2\Sigma^+$ and $^2\Sigma^-$ states in relation to the ground state curves of HCO and HCO^+, as functions of R(C–O); (*a*) $\measuredangle$HCO = 180°; (*b*) $\measuredangle$HCO = 140°.

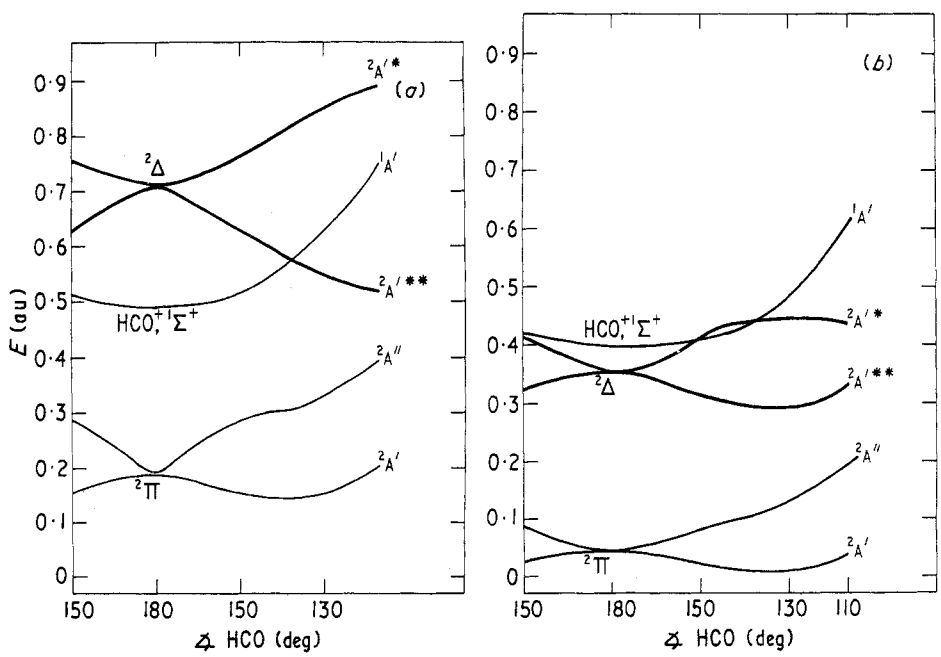

Figure 3. Sections through the potential surfaces showing the behaviour of the ground states of HCO and HCO^+ and the $^2\Delta$ state of HCO, as the $\measuredangle$HCO is varied; (*a*) R(C–O) = 1·00 Å; (*b*) R(C–O) = 130 Å.

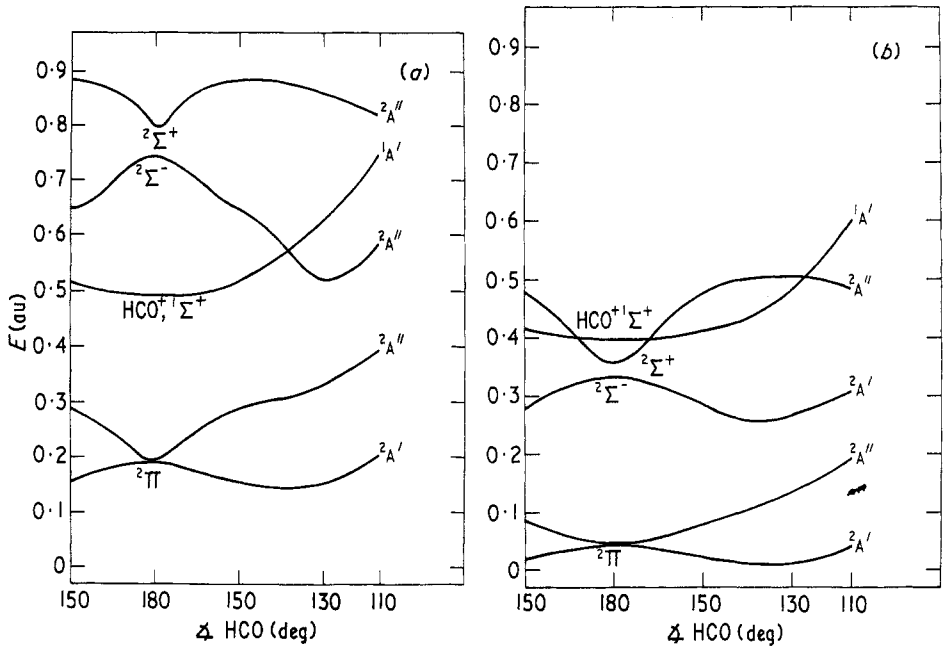

Figure 4. Sections through the potential surfaces showing the behaviour of the ground states of HCO and HCO^+ and the $^2\Sigma^-$ and $^2\Sigma^+$ states of HCO, as the ∡HCO is varied; (*a*) *R*(C–O) = 1·00 Å; (*b*) *R*(C–O) = 1·30 Å.

(Dixon 1969) ∡ HCO = 123·8° and *R*(C–H) = 1·16 Å. However, the calculated vertical transition energy from the ground $^2\Pi(^2A')$ state to the $^2\Pi(^2A'')$ state is about 1·5 eV greater than the observed value. We have assumed that the shapes of the surfaces are correct in the regions around their minima and have arbitrarily moved the curves vertically to make the energy intervals correspond to the experimental spectra.

From the potential surfaces, we can find the crossing regions where LZS transition probability for ionization of particular states of HCO can accumulate or, alternatively where the electron leaves, in the model based on unit probability for chemi-ionization at the creases. A diagram of the crossing regions for each state is shown in figure 5; these regions are actually almost sectors of spheres for three of the four states. The finite width of the shells in the figure is supposed to indicate the transition probability between the two states in the LZS approximation.

The interaction energy, $\epsilon_{if}(R_0)$, was assumed to be equal to the interaction energy between the $B'^2\Delta$ state and the $N^2\Delta$ Rydberg state of the isoelectronic NO molecule (Telenbok and Lefebvre-Brion 1966, Bardsley 1968). The most probable value given to $\epsilon_{if}(R_0)$ is 0·052 eV (Telenbok and Lefebvre-Brion 1966) which is assumed constant for all angles and the three intereacting molecular states. Because of the approximations inherent in this assumption a range of 0·06 eV was chosen about 0·052 eV. This range was covered in three steps 0·022, 0·052 and 0·082 eV and was thought to be sufficiently large to incorporate the true value of $\epsilon_{if}(R_0)$, which, at present, is unknown.

When this work was begun, the position of the HCO molecular states relative to the $HCO^+ {}^1\Sigma^+(^1A')$ ground state was not well determined. Hence our calculations were carried out initially for three different energies of the HCO excited-state surfaces, relative to the surface for HCO^+. The minimum of the HCO^+ curve is located to correspond with

Warneck's value of 4 kcal for the exothermicity of the reaction. The curves are illustrated in figure 6. The surface B was chosen so that the energy of the crossing point in the linear configuration was equal to the energy of $CH(X^2\Pi)+O(^3P)$. The curves A and C were then constructed by displacing the explicitly computed part of curve B by $+0{\cdot}05$ au

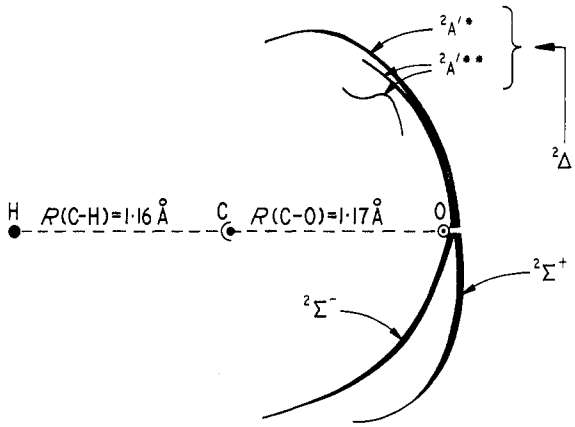

Figure 5. The interaction or 'surface-crossing' regions of various excited states of HCO with the ground state surface for $HCO^+ + e$. The C–H distance is held fixed; each arc or curve is a section of the surface of revolution of the intersection of the potential surface of that particular state of HCO with the surface for HCO^+, when the C–O distance and the HCO angle are varied. The $^2\Delta$ state splits for $\angle HCO < 180°$, into $^2A'^*$ and $^2A'^{**}$; the surface of $^2A'^{**}$ cuts the surface for HCO^+ ($^1A'$) in two unconnected regions, as shown. The equilibrium R(CO) of 1·17 Å is also indicated for the linear molecule-ion. The width of the shading is proportional to the transition probability.

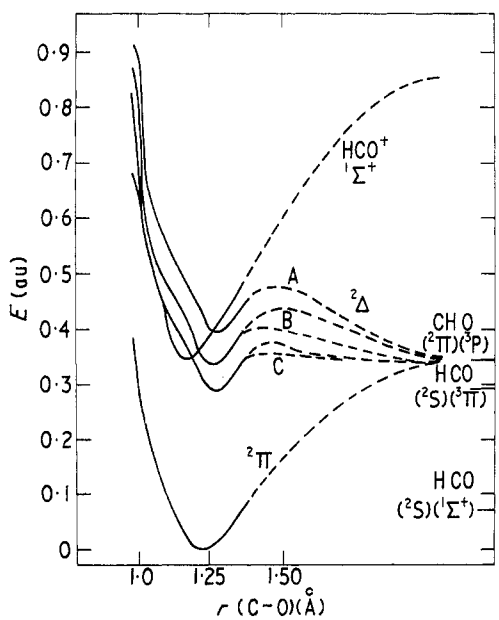

Figure 6. Various choices of potentials for the $^2\Delta$ excited state of HCO, as functions R(C–O). (Shown for linear HCO only.)

and −0·05 au respectively. B probably corresponds most closely to reality, but the others, and particularly C, must be considered real possibilities. We have also tried using the curve shapes that correspond to reasonable upper and lower limits on the activation barriers for the $^2\Delta$ and $^2\Sigma^-$ states, consistent with our INDO calculations. The upper limits of the activation barriers are based on the INDO values of the energy at the largest C–O distances for which the solid curves are drawn. These are the distances for which the calculation is least reliable. The lower limits were obtained by neglecting the outermost computed points and assuming that the potentials go monotonically from their values at the next-outermost computed point to infinity. This assumption makes the $^2\Sigma^-$ state show no activation energy for any HCO angle; the $^2\Delta$ state has an activation energy in its linear configuration even with this assumption, but when the molecule is bent, the activation energy goes rapidly to zero. These are shown in the outer parts of the potentials of figures 1 and 2. No attempt was made to estimate the effects of varying the activation energy for the $^2\Sigma^+$ state (figure 2) because this state contributes so little to the cross section.

A further investigation was made of the effect of different values of the coupling parameter or interaction energy $\epsilon_{if}(R_0)$. Transition probabilities for each trajectory were calculated using the LZS equation with $\epsilon_{if}(R_0)$ varying between 0·022 eV and 0·082 eV. The cross sections as a function of $\epsilon_{if}(R_0)$ are shown in figure 7 where the curve

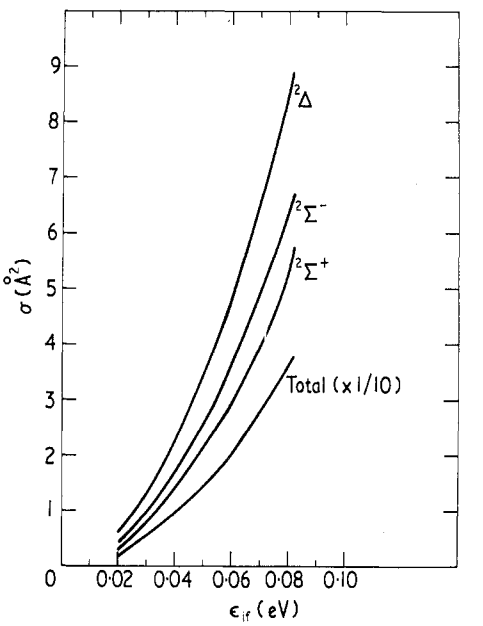

Figure 7. Reaction cross sections as functions of the interaction energy ϵ_{if} for a collision energy of 0·1 au or 2·72 eV. These curves are based on the choice of curve B for the $^2\Delta$ state and the lower activation barrier in all cases.

labeled 'total' is calculated from $\sigma(\epsilon_{if}) = \Sigma_{j=1}^{n} G_j \sigma_j(\epsilon_{if})$. The statistical weight of the ith state is G_i; since the total weight for $^2\Pi + {}^3P$ is 36, the $^2\Sigma^-$ and $^2\Sigma^+$ each have $G_i = \frac{1}{18}$, while $^2\Delta$ has $G_i = \frac{1}{9}$.

Cross sections for each state and the total cross section as a function of collision energy are depicted in figures 8–11. These curves are for $\epsilon_{if}(R_0) = 0{\cdot}05$ eV. As can be

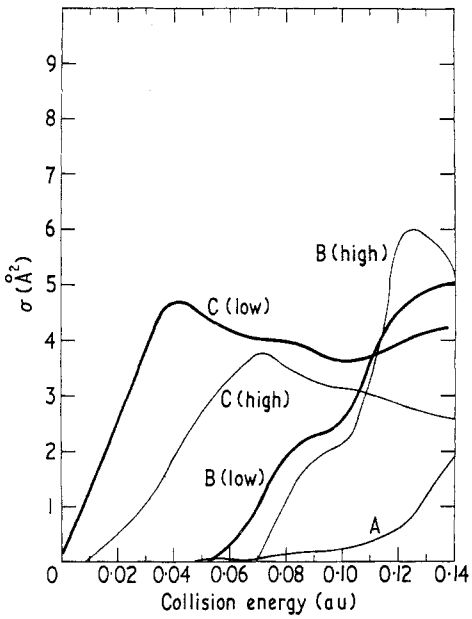

Figure 8. Cross section for formation of $HCO^+ + e$ from CH + O, via the $^2\Delta$ state of HCO. Interaction energy ϵ_{if} is taken as 0·052 eV; the letters correspond to the choices shown in figure 6; 'high' and 'low' refer to the higher and lower activation barriers shown in figure 6.

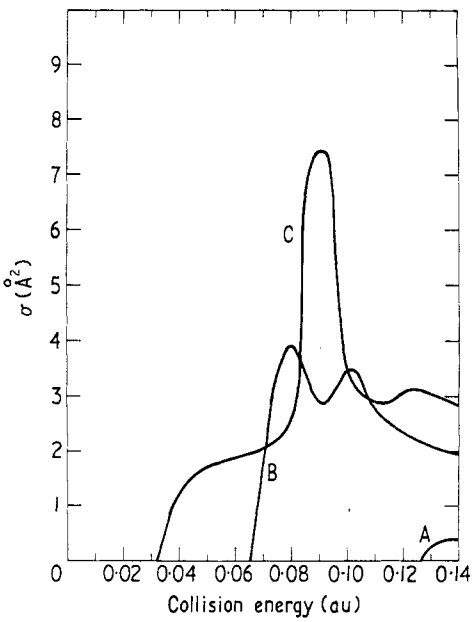

Figure 9. Cross section for formation of $HCO^+ + e$ via the $^2\Sigma^+$ state of HCO, with $\epsilon_{if} = 0{\cdot}052$ eV. Choices A, B and C correspond to placement of the solid portions of the $^2\Sigma^+$ surface at an energy 0·05 au higher than that shown in figure 2, at the energy shown in figure 2, and at an energy 0·05 au below that shown in figure 2.

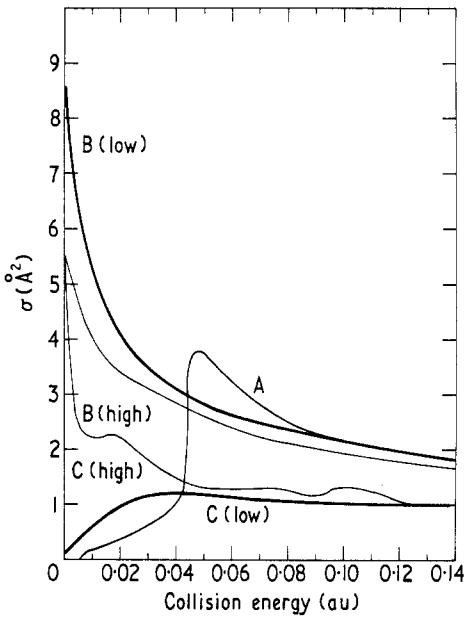

Figure 10. Cross sections for formation of $HCO^+ + e$ via the $^2\Sigma^-$ state of HCO, with $\epsilon_{if} = 0{\cdot}052$ eV. Choices A, B and C are chosen as indicated previously; B indicates the surface as shown in figure 2, while A and C indicate trial surfaces with their solid portions 0·05 au higher and lower, respectively, than is shown in figure 2; 'low' and 'high' indicate the choices of activation barriers in the outer dashed portion of the curves shown in figure 2.

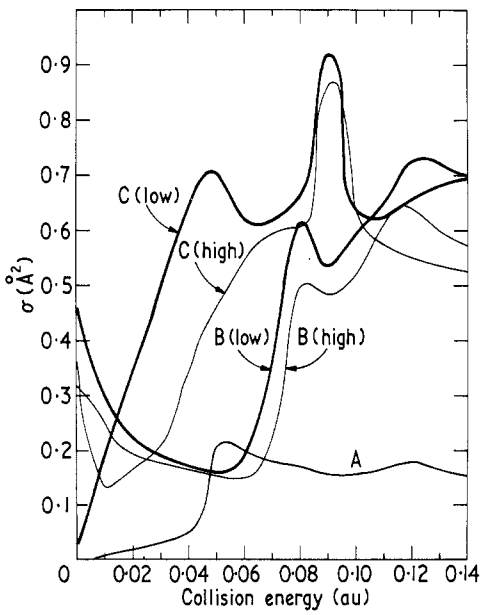

Figure 11. Total cross sections for formation of $HCO^+ + e$ from the $^2\Delta$, $^2\Sigma^+$ and $^2\Sigma^-$ states of HCO. Choices A, B and C, and 'low' and 'high' have the same meanings as in the previous figures on which this figure is based.

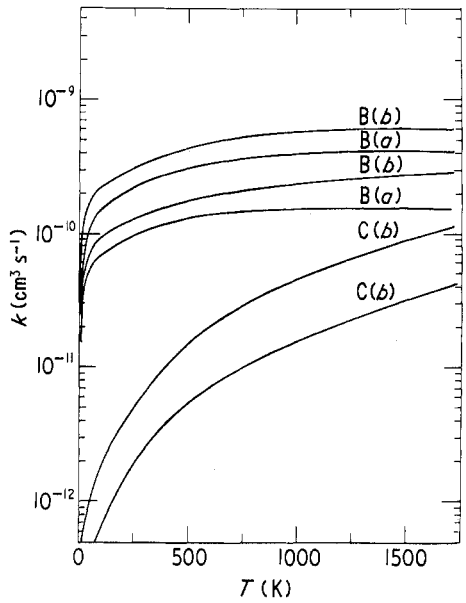

Figure 12. Rate coefficient as a function of temperature for formation of $HCO^+ + e$ from $CH + O$ via the $^2\Sigma^-$ state of HCO. The top two curves are drawn for $\epsilon_{if} = 0{\cdot}082$ eV, and the rest, for $\epsilon_{if} = 0{\cdot}052$ eV. B and C have meanings as before; (*a*) and (*b*) indicate higher and lower choices of activation barriers, respectively.

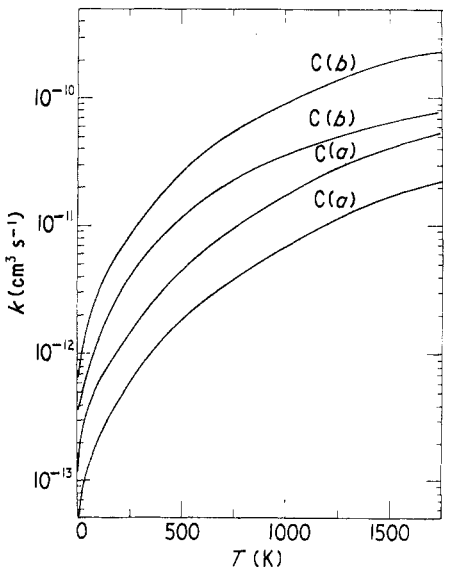

Figure 13. Rate coefficient, as a function of temperature, for the formation of $HCO^+ + e$ via the $^2\Delta$ state of HCO. Reading from top down, curves are drawn for $\epsilon_{if} = 0{\cdot}082$ eV, 0·052 eV, 0·082 eV and 0·052 eV; all curves in this figure are drawn for choice C of the curves in figure 6, and (*a*) and (*b*) refer to the higher and lower choices of activation barriers.

seen from figure 10, the $^2\Sigma^-$ state is the only one which will contribute to the reaction at the very low temperatures which occur in interstellar space. All three states can contribute to the reaction in flames; even in the atomic oxygen–hydrocarbon flames at room temperature, there is a considerable cross section for this reaction. The rate constant as a function of temperature has been calculated for specific states and is shown in figures 12 and 13 for different values of $\epsilon_{if}(R_0)$ and positions of the potential energy surfaces. The total LZS rate is shown, for a wide variety of parameters, in figure 14.

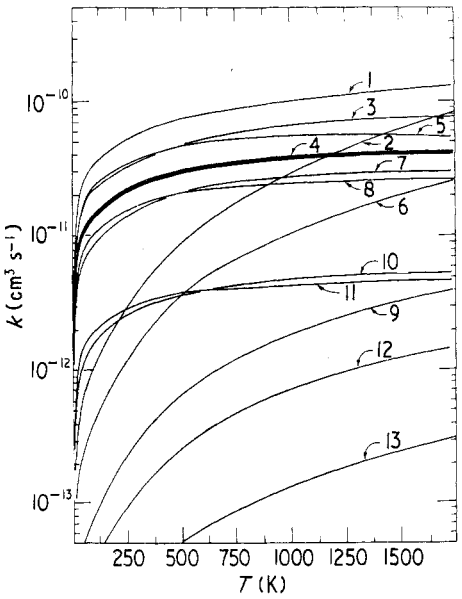

Figure 14. Total rate coefficient for formation of HCO^+ from CH+O, as a function of temperature. Curves are numbered to correspond to the parameter sets indicated below. The indications A, B and C refer to the choices of potentials shown in figure 6 and, for potential sets B and C, figure 10 as well. The curves corresponding to cases B and C in this figure were based on the *low* activation energy model: zero activation energy for the $^2\Sigma^-$ surface for all HCO angles, and zero activation energy on the lower $^2\Delta(A')$ surface for large HCO angles. The curve we consider the best working choice is curve 4, drawn heavily; curves 3, 5, 7 and perhaps 1 and 8 can also be considered reasonably likely. The others, with the exception of curves 9, 12 and 13, must be considered possible but not likely; the lowest curves, 9, 12 and 13 are included only to illustrate the effect that a long-range repulsive surface, such as A, would have on that rate. It is worth noting that the rates were also computed for the corresponding curves but with high activation energies as shown in figure 6. The principal effect of the barrier is to turn the curves sharply downward for temperatures below 500 K. Curve 4, in the high barrier case, gives $k \sim 10^{-12}$ cm^3 s^{-1} at 250 K and 10^{-14} at 125 K, and the other rates so calculated are correspondingly low at low temperatures, as one would expect.

Parameter Sets:

1. B(b) ϵ_{if} = 0·082
2. C(b) ϵ_{if} = 0·082
3. B(a) ϵ_{if} = 0·082
4. B(b) ϵ_{if} = 0·052
5. C(a) ϵ_{if} = 0·082
6. C(b) ϵ_{if} = 0·052
7. B(a) ϵ_{if} = 0·052
8. C(a) ϵ_{if} = 0·052
9. A(a) ϵ_{if} = 0·082
10. B(a) ϵ_{if} = 0·022
11. C(a) ϵ_{if} = 0·022
12. A(a) ϵ_{if} = 0·052
13. A(a) ϵ_{if} = 0·022

Because the chemi-ionization reaction of CH + O may play an important role in the formation of interstellar molecules, it is useful to examine explicitly the values of the rate coefficients for specific states and for the total reaction, at temperatures of 3 °K and 25 °K. These rates are given in table 1, for the most probable sets of parameters.

Table 1. Rate coefficients (in $cm^3\ s^{-1}$) for $HC + O \rightarrow HCO^+ + e$ for specific states and various choices of potentials and interaction matrix elements, at 3 K and 25 K.

	3 K	25 K
$^2\Sigma^-$ *State:* (G_i excluded)†		
$\epsilon_{if} = 0{\cdot}08$ eV, low barrier	$4{\cdot}3 \times 10^{-11} cm^3\ s^{-1}$	$1{\cdot}4 \times 10^{-10} cm^3\ s^{-1}$
$\epsilon_{if} = 0{\cdot}08$ eV, high barrier	$2{\cdot}7 \times 10^{-11}$	$7{\cdot}5 \times 10^{-11}$
$\epsilon_{if} = 0{\cdot}05$, low barrier	$1{\cdot}7 \times 10^{-11}$	$5{\cdot}0 \times 10^{-11}$
$\epsilon_{if} = 0{\cdot}05$, low barrier	$1{\cdot}2 \times 10^{-11}$	$3{\cdot}5 \times 10^{-11}$
$^2\Delta$ *State*‡		
$\epsilon_{if} = 0{\cdot}08$, low barrier	$4{\cdot}4 \times 10^{-12}$	$1{\cdot}2 \times 10^{-11}$
$\epsilon_{if} = 0{\cdot}05$, low barrier	$2{\cdot}1 \times 10^{-12}$	$6{\cdot}0 \times 10^{-12}$
$\epsilon_{if} = 0{\cdot}08$, high barrier	$9{\cdot}0 \times 10^{-14}$	$2{\cdot}6 \times 10^{-13}$
$\epsilon_{if} = 0{\cdot}05$, low barrier	$3{\cdot}2 \times 10^{-14}$	$9{\cdot}0 \times 10^{-14}$
Case§		
1: low barrier, $\epsilon_{if} = 0{\cdot}082$	$6{\cdot}0 \times 10^{-12}$	$1{\cdot}7 \times 10^{-11}$
3: high barrier, $\epsilon_{if} = 0{\cdot}082$	$4{\cdot}1 \times 10^{-12}$	$1{\cdot}2 \times 10^{-11}$
4: low barrier, $\epsilon_{if} = 0{\cdot}052$	$2{\cdot}4 \times 10^{-12}$	$7{\cdot}0 \times 10^{-12}$
7: high barrier, $\epsilon_{if} = 0{\cdot}052$	$1{\cdot}0 \times 10^{-12}$	$4{\cdot}4 \times 10^{-12}$
10: high barrier, $\epsilon_{if} = 0{\cdot}022$	$3{\cdot}0 \times 10^{-13}$	$9{\cdot}0 \times 10^{-13}$

† The values of ϵ_{if} for the $^2\Sigma^-$ state also refer to surface B of figure 10.
‡ All values based on curve C of figure 6, to indicate the largest reasonable contribution that this state may make, rather than curve B, which is more likely to represent the real state; both curve B and curve C were used to calculate the values of the total rate given below. Degeneracy factor is omitted.
§ Total rate for the cases of most probably behaviour, all based on curves B. Cases are numbered to correspond to the indices of the curves in Figure 14. Case 4, with curves B for the $^2\Sigma^-$ and $^2\Delta$ states, a minimal activation barrier and $\epsilon_{if} = 0{\cdot}05$, is, in our judgement, a best estimate based on present evidence.

The cross sections for the two most important states ($^2\Delta$ and $^2\Sigma^-$) and the total cross section, for the unit probability model, are given in figure 15. These are clearly large compared with the LZS cross sections. Correspondingly, the rate coefficients for the individual states and for the total reaction are considerably larger than for the LZS case, as figure 16 shows.

The rate of this reaction has been estimated previously on several occasions. A calculation via microscopic reversibility was performed on the isoelectronic reaction $N + O \rightarrow NO^+ + e^-$, giving a value of $5 \times 10^{-12}\ cm^3\ s^{-1}$ (Bascombe *et al* 1962) and the experimental evaluation of the rate in methane flames gave a value of $3 \times 10^{-12}\ cm^3\ s^{-1}$, (Peeters *et al* 1969). These two results are certainly within our error limits, and fit well with our most favoured curve in figure 14. Other values (cf Fontijn 1965, Peeters 1969) span the range from $3 \times 10^{-13}\ cm^3\ s^{-1}$ to 1×10^{-11}; the latter value is based on a theoretical model similar to our unit probability model. A more thorough *ab initio* investigation of the position of the potential energy curves and an exact calculation of $\epsilon_{if}(R_0)$ would be appropriate now and some preliminary computations have been done

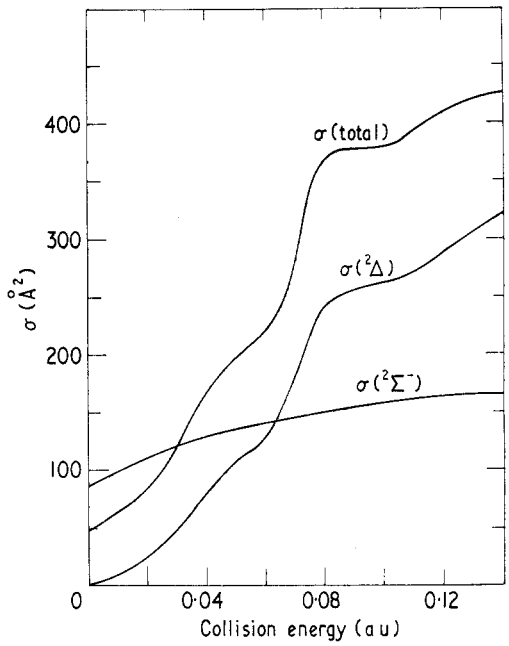

Figure 15. Energy dependence of the cross sections for the $^2\Sigma^-$ state, the $^2\Delta$ state and for the total reaction when the probability of reaction is unity for all trajectories passing the surface crossing. Surface parameters are B(b), $\epsilon_{if} = 0{\cdot}052$ eV.

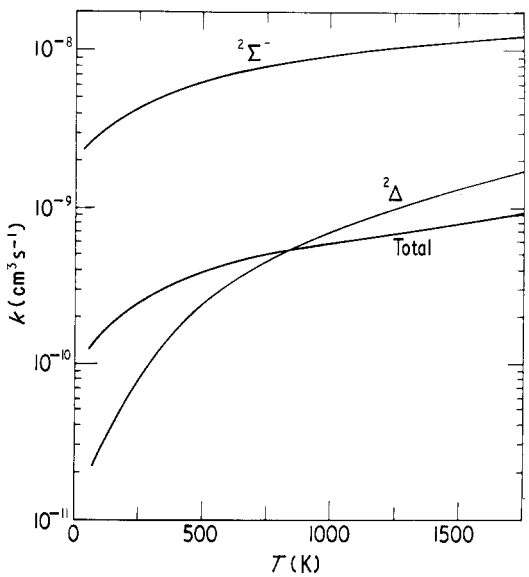

Figure 16. Rate coefficients for the $^2\Sigma^-$ state, the $^2\Delta$ state and the total reaction, according to the unit probability model. Surface parameters are the same as for figure 15.

toward this goal. Such calculations will hopefully fix the rate curve more accurately and validate our INDO results which are obviously easier to apply to other systems, if their accuracy justifies their use. The *ab initio* results thus far do indicate that the shapes of the INDO curves are correct.

The fact that quite a substantial rate over a large range of temperature was obtained proves fairly conclusively that the reaction $CH + O \rightarrow HCO^+ + e^-$ can indeed be the primary ion-forming reaction in hydrocarbon–oxygen atom flames. This rate should be most helpful in determining many of the other unknown kinetic parameters of flame ionization and possibly lead to a determination of the ionization mechanism and a better understanding of flame processes.

References

Bardsley J N 1968 *J. Phys.* B: *Atom. molec. Phys.* **1** 365

Bascombe K N, Green J A and Sugden T M 1962 *Joint Symposium on Mass Spectrometry–ASTM and Institute of Petroleum* (Oxford: Pergamon Press)

Bates D R 1960 *Proc. R. Soc.* A **257** 22

Buhl D and Snyder L E 1970 *Nature* **228** 267

Coulson C A and Zalewski K 1962 *Proc. R. Soc.* A. **268** 437

Dixon R N 1969 *Trans. Faraday Soc.* **65** 3141

Dressler K and Miescher E 1965 *Astrophys. J.* **141** 1266

Fontijn A, Miller W J and Hogan J M 1965 *X Int. Symp. on Combustion* (Pittsburgh Pa: Combustion Institute) p 545

Huzinaga S and Arnau C 1970 *Phys. Rev.* A **1** 1285

—— 1971 *J. chem. Phys.* **54** 1948

Johns J W C, Priddle S H and Ramsay D A 1960 *Disc. Faraday Soc.* **35** 90

Klemperer W 1970 *Nature* **227** 1230

Landau L and Lifshitz E M 1958 *Quantum Mechanics* (Oxford and Paris: Pergamon Press)

Lawton J and Weinberg F 1964 *Proc. R. Soc.* **227** 468

Matsuda S and Gutman D 1970 *J. chem. Phys.* **53** 3324; **54** 453

Matthews C S and Warneck P 1969 *J. chem. Phys.* **51** 854

Milligan D E and Jacox M E 1969 *J. chem. Phys.* **51** 277

Olson R E, Smith F T and Bauer E 1971 *Appl. Optics* **10** 1848

Peeters J and Van Tiggelen A 1969 *XII Int. Symp. International on Combustion* (Pittsburgh Pa: Combustion Institute) p 969

Peeters J, Vinckier C and Van Tiggelen A 1969 *Oxidation and Combustion Reviews* **4** 93

Peeters J, Lambert K F, Hertoghe P and Van Tiggelen A 1971 *XIII Int. Symp. on Combustion* (Pittsburgh Pa: Combustion Institute) p 321

Pople J A and Beveridge D L 1970 *Approximate Molecular Orbital Theory* (New York: McGraw-Hill)

Shirk J S and Pimentel G C 1968 *J. Am. Chem. Soc.* **90** 3349

Stueckleberg E G C 1932 *Helv. Phys. Acta* **5** 369

Telenbok P and Lefebvre-Brion H 1966 *Can. J. Chem.* **44** 1677

Tully J and Preston R C 1971 *J. chem. Phys.* **55** 562

Zener C 1932 *Proc. R. Soc.* A **137** 696